Journal of Materials Chemistry A

PAPER

Check for updates

Superaerophobic hydrogels for diaphragm modification to suppress gas crossover in alkaline water electrolyzers

Soi Lee, [ID] [ab] Jinseo Lee, [ID] [ab] Seunghyun Lee, [ID] [a] Hyeongoo Kim, [ID] [ab] Yunseok Kang, [ID] [ab] Dong Woog Lee [ID] [a] and Jungki Ryu [ID] *[abcd]

Among low-temperature electrolyzer technologies, alkaline water electrolysis (AWE) is the most mature owing to its durability and reliance on inexpensive materials. However, AWEs still face safety concerns arising from gas crossover through porous diaphragms, which can lead to hydrogen accumulation in the oxygen stream and potential explosion risk. Suppressing gas crossover is therefore essential for the safe and scalable deployment of AWE systems. Herein, we present a strategy to control diaphragm wettability using superaerophobic polyvinyl alcohol (PVA) hydrogel coatings that mitigate gas crossover. Gas transport across the diaphragm was quantified through a combination of (i) penetrated oxygen assessment *via* H-cell oxygen reduction reaction (ORR) current analysis and (ii) direct dissolved oxygen measurements during AWE operation. In addition, gas chromatography analysis of the anode gas phase was performed to directly verify hydrogen crossover. These complementary measurements consistently demonstrate a reduced crossover rate enabled by the hydrogel's superaerophobicity. *In situ* visualization further reveals rapid bubble detachment from the hydrogel-coated surface, preventing pressure buildup and suppressing bulk gas penetration. Overall, this study introduces a simple, energy-efficient diaphragm modification strategy that directly addresses a key safety challenge in AWE. By improving gas management without compromising electrochemical performance, this approach offers a practical pathway toward safer and more reliable alkaline water electrolysis for industrial hydrogen production.

1. Introduction

Production of green hydrogen by water electrolysis powered by renewable electricity is a key enabler of the transition toward a sustainable society.[1–6] Hydrogen is highly versatile, serving both as a clean fuel[7] and as a chemical feedstock,[8] yet it is still predominantly produced from fossil fuels,[9] resulting in massive CO_2 emissions. Although water electrolysis is among the simplest and most extensively studied electrochemical reactions, it remains highly challenging and requires the development of multiple functional components, including catalysts, membranes/separators, ionomers, and porous transport layers. Each of these components has diverse material options and can be integrated into different types of electrolyzers, ranging from conventional alkaline systems to next-generation

designs such as proton exchange membrane (PEM),[10] anion exchange membrane (AEM),[11] and bipolar membrane (BPM)[12] electrolyzers. Among these, alkaline water electrolyzers (AWEs) equipped with thick, porous diaphragms have long been commercialized owing to their relatively simple architecture and the use of inexpensive materials.[13,14] However, they generally suffer from low energy efficiency and limited hydrogen production rates, even when operated in highly concentrated alkaline solutions.[15,16] Next-generation electrolyzers based on thin ion-selective membranes can mitigate some of these issues[17–23] and, in principle, operate with pure water.[24,25] Nevertheless, their practical deployment is hindered by the reliance of PEM electrolyzers on expensive noble metals[26] (*e.g.*, Pt and Ir) and the chemical instability of AEMs and BPMs (particularly quaternary ammonium groups under alkaline conditions).[27,28] Furthermore, operation with pure water typically results in diminished performance and accelerated membrane degradation.[29,30]

In this context, many researchers have revisited AWEs to address the urgent demand for green hydrogen production in achieving carbon neutrality.[31–33] Although AWEs often exhibit lower performance due to their thick, porous diaphragms, they demonstrate greater durability because ion transport occurs physically through pores rather than *via* chemically reactive

[a]School of Energy and Chemical Engineering, Ulsan National Institute of Science and Technology (UNIST), Ulsan 44919, Republic of Korea. E-mail: jryu@unist.ac.kr

[b]Emergent Hydrogen Technology R&D Center, Ulsan National Institute of Science and Technology (UNIST), Ulsan 44919, Republic of Korea

[c]Graduate School of Carbon Neutrality, Ulsan National Institute of Science and Technology (UNIST), Ulsan 44919, Republic of Korea

[d]Center for Renewable Carbon, Ulsan National Institute of Science and Technology (UNIST), Ulsan 44919, Republic of Korea

functional groups.[13,34,35] However, AWEs are prone to gas crossover through diaphragm pores. Gas bubbles generated between the electrodes and the diaphragm increase local pressure gradients, thereby accelerating gas crossover.[36–39] The gas crossover issue becomes particularly critical at low current densities relevant to the operation with renewable power sources.[40–42] Under such conditions, the gas generation rate may become comparable to or even lower than the gas permeation rate across the separator. As a result, hydrogen can accumulate in the oxygen stream, leading to safety concerns, since hydrogen concentrations above 4 vol% in oxygen can form explosive mixtures.[37,43] In practical electrolyzer operation, much stricter safety thresholds are typically applied, and the system is controlled to shut down or limit operation when the hydrogen-in-oxygen ratio (HTO) in the gas phase approaches about 2 vol% to prevent explosion risks and ensure safe operation.[44] Nevertheless, conventional AWE research has predominantly focused on catalyst development to reduce kinetic overpotentials, often overlooking the critical issues of gas crossover through diaphragms.[45–47] Although interest in diaphragm materials has increased recently, most studies have emphasized electrochemical performance improvements. Moreover, many such approaches rely on expensive or hazardous materials, or require complex and time-consuming fabrication processes (Table S1, SI). Consequently, systematic studies employing safe, cost-effective strategies to suppress gas crossover at the electrode–separator interface remain limited.

Herein, we report a superaerophobic polyvinyl alcohol (PVA) hydrogel coating on Zirfon diaphragms as a simple strategy to suppress gas crossover in AWEs, particularly under high current density conditions. The chemically crosslinked hydrogel forms a robust, porous, and hydrophilic network that effectively repels gas bubbles and reduces dissolved gas permeation under harsh alkaline and high-temperature conditions. A diaphragm coated with an optimal hydrogel loading significantly suppressed gas crossover, as evidenced by reduction in ORR current in an H-cell and a marked decrease in dissolved oxygen concentrations during electrolysis. Gas chromatography further confirmed effective suppression of hydrogen crossover, with HTO values of 0.69% at 10 mA cm^{-2} and 0.22% at 1000 mA cm^{-2} after 2 h of AWE operation, both well below the typical industrial safety threshold (~2 vol%). These findings highlight interfacial wettability engineering as a critical design principle for diaphragm design and demonstrate a practical, durable, and cost-effective route to improve both safety and efficiency in alkaline water electrolysis.

2. Experimental

2.1. Materials

Ni foam (thickness: 1.6 mm) was purchased from MTI Korea (Korea). Carbon cloth was obtained from Fuel Cell Earth. Polypropylene mesh (PP mesh, 0.025″ × 0.030″) and 5 wt% PiperION dispersion and 20 wt% Pt/Vulcan XC-72 carbon was purchased from Fuel Cell Store (USA). ZrO$_2$ nanopowder (20–30 nm) was purchased from UniNanoTech (Korea). N-Methyl-2-pyrrolidone (NMP, ≥99%), polysulfone (PSU, M_w ~35 000),

polyvinyl alcohol (PVA, M_w 89 000–98,000), glutaraldehyde (50 wt% in H$_2$O), H$_2$SO$_4$ (95.0–98.0%), Ni(SO$_4$)·6H$_2$O (≥98%), Fe(NO$_3$)$_3$·9H$_2$O (≥98%), ethanol (≥99.5%), and KOH (≥85%) were purchased from Sigma-Aldrich (USA). RANEY® Ni (slurry in H$_2$O) was obtained from TCI Chemicals (Japan). Nafion solution was purchased from Omniscience (Korea).

2.2. Preparation of diaphragms

The casting slurry for the diaphragm was prepared by dissolving PSU (15 wt%) in NMP at 50 °C under mild stirring for over 6 h.[48] ZrO$_2$ nanopowder (85 wt%) was then added to the PSU solution and mixed under continuous stirring. A PP mesh was cleaned by sonication in ethanol for 10 min, followed by rinsing with deionized (DI) water and drying under nitrogen flow. The slurry was cast onto the cleaned PP mesh using a doctor-blade technique.[49,50] The resulting diaphragm was immersed in DI water for 5 min for phase inversion and subsequently washed several times to remove residual solvent following previous report.[37] The final thickness of the diaphragm was approximately 500 μm. PVA solutions at concentrations of 2, 4, and 6 wt/v% were prepared by dissolving PVA in 0.5 M H$_2$SO$_4$ at 85 °C until complete dissolution, following a reported procedure.[51] The hydrogel-coated diaphragm was fabricated by dipping the above diaphragm into the PVA solution for 1 min, followed by crosslinking in a 10 v/v% glutaraldehyde solution for 1 min.

2.3. Characterizations

The diaphragms were freeze-dried overnight prior to morphology analysis. Surface morphology was analyzed using a Hitachi SU-7000 SEM (Japan). Air contact angles were measured with a drop shape analyzer (DSA 100, KRÜSS, Germany) using a 6 μL air bubble. FT-IR spectroscopy was performed in attenuated total reflectance (ATR) mode using a 670-IR spectrometer (Varian Instruments, USA). Confocal laser scanning microscopy (CLSM; ZEISS LSM 980, Germany) was used to measure hydrogel thickness of the hydrogel coating, with the hydrogel layer stained for imaging. Bubble adhesion forces were measured with a micro-tensiometer system after forming an air bubble on the surface. Bubble point pressure (BPP) was determined using a custom-built cell. Porosity and pore distribution of PVA hydrogel were calculated using in-house software. The *in situ* behavior of hydrogen bubble was observed using a high-speed camera (Fastcam Mini UX50, Photron, Japan).

2.4. Preparation of electrocatalysts

Ni foam was compressed to a thickness of 400 μm to prepare the HER catalyst. The casting solution was prepared by mixing RANEY® Ni slurry with Nafion solution in a DI water/ethanol mixture, as described in a previous study.[52] The solution was then sonicated for more than 1 h. and drop-casted onto pressed Ni foam at 60 °C, with a loading of ~0.01 g cm^{-2}. The deposited catalyst was dried in a vacuum oven overnight. NiFe catalysts were deposited on Ni foam by electrodeposition following previous literature.[53] A three-electrode cell was used with Ni foam, Ag/AgCl, and Ni foil as the working, reference, and

counter electrodes, respectively. In an electrolyte containing 3 mM $Ni(SO_4)\cdot6H_2O$ and 3 mM $Fe(NO_3)_3\cdot9H_2O$, chronoamperometry was performed under -1 V vs. Ag/AgCl for 5 min. The deposited electrodes were rinsed with DI water and dried under nitrogen flow.

2.5. AWE cell assembly

An AWE cell with an active area of 5 cm^2 and integrated flow fields was used. Polytetrafluoroethylene (PTFE) gaskets (200 µm thickness) were employed to seal the cell. A 30 wt% KOH solution, preheated to 80 °C, served as the electrolyte. The electrolyte was circulated through both anode and cathode compartments at a flow rate of 50 mL min^{-1}.[54]

2.6. Electrochemical characterizations

All electrochemical analyses were conducted using a SP-300 potentiostat/galvanostat (Bio-Logic Science Instruments, France) without iR compensation. Linear sweep voltammetry (LSV) was conducted at a scan rate of 10 mV min^{-1}. OH^- conductivity was calculated from potentiostatic electrochemical impedance spectroscopy (PEIS) at -0.3 V vs. the reversible hydrogen electrode (RHE) over a frequency range of 100 kHz to 1 Hz. Galvanostatic electrochemical impedance spectroscopy (GEIS) of AWE was measured at 1000 mA cm^{-2} over a frequency range of 5 kHz to 100 mHz.

2.7. Gas crossover measurements

Gas crossover across diaphragms with and without hydrogel modification was investigated using three complementary methods: (1) indirect measurement of reduction current densities in an H-cell, with continuous H_2 and O_2 purging to the cathode and anode compartments, respectively; (2) direct measurement of dissolved oxygen (DO) concentrations in electrolytes in both anode and cathode compartments before and after AWE operation at room temperature using a DO sensor; and (3) measurement of hydrogen-in-oxygen ratio (HTO) from the outlets of an AWE operated at 80 °C.

(1) Measurement of reduction current densities in an H-cell: chronoamperometry (CA) was conducted at 0.2 V vs. RHE to evaluate the ORR current arising from penetrated O_2 in an H-cell at room temperature. A Pt/C electrode (0.5 cm^2), a NiFe electrode (0.8 cm^2), and a Hg/HgO electrode were used as the working, counter, and reference electrodes, respectively. During the measurement, pure N_2 and O_2 gases were continuously purged into the working and counter electrodes compartments, respectively.

(2) Measurement of DO concentration in an AWE: to quantify DO, chronopotentiometry (CP) was performed at 10 mA cm^{-2} and 1000 mA cm^{-2} for 30 min in an AWE cell at room temperature. Prior to the reaction, the catholyte and anolyte were purged with inert gas at least 30 min to minimize DO concentration in the electrolyte. After the reaction, DO concentrations in both catholyte and anolyte were measured using a pH/DO multiparameter Meter (Orion Star A216, Thermo Fisher Scientific, USA) equipped with a DO probe (Orion 083005MD, Thermo Fisher Scientific, USA).

(3) Measurement of hydrogen-in-oxygen ratio (HTO) from an AWE: the HTO in the anode gas phase was determined during CP at 10 mA cm^{-2} and 1000 mA cm^{-2} in an AWE cell system operated at 80 °C. Prior to the reaction, both the catholyte and anolyte were purged with pure N_2 gas for at least 30 min to remove dissolved gases from the electrolyte. During operation, the HTO values were monitored using gas chromatography (Shimadzu 2010 Plus, Shimadzu, Japan).

3. Results and discussion

3.1. Preparation and characterization of PVA hydrogel-modified diaphragms

We hypothesize that hydrogel modification of porous diaphragms can effectively suppress gas crossover in alkaline water electrolyzers (Fig. 1). While the pores of a diaphragm facilitate the conduction of OH^- ions, they can also allow hydrogen and oxygen molecules to permeate across the diaphragm, resulting in safety concerns and reduced hydrogen purity.[55] Gas crossover through pores may occur via two pathways: (1) the transport of gas bubbles and (2) the molecular diffusion of dissolved gases. In practical electrolysis, the vast majority of gases are present as bubbles because H_2 and O_2 production rates (~18.7 and ~9.35 mmol cm^{-2} h^{-1} at 1 A cm^{-2}, respectively) are much higher than their solubility (0.8 and ~1.2 mmol). Recently, our group demonstrated that hydrogel overlayer can promote bubble detachment from electrode surfaces due to their superaerophobicity, thereby significantly improving electrolysis performance.[56–60] In addition, Feng and coworkers reported that gas permeation through hydrogel membranes is substantially lower than through water, as water molecules bound with hydrogels reduce effective gas solubility.[61] Motivated by these findings, we hypothesize that modifying diaphragms with porous hydrophilic hydrogels can suppress gas crossover during water electrolysis by preventing bubble adhesion on diaphragm surfaces and hindering gas diffusion through diaphragm pores.

Porous diaphragms for alkaline water electrolyzers were coated with superaerophobic hydrogels by chemically cross-linking PVA (Fig. 2a). We specifically tested the modification of Zirfon diaphragms which are widely used in commercial alkaline water electrolyzers. Zirfon diaphragms were fabricated by coating a polypropylene mesh with ZrO_2 nanopowders and polysulfone via doctor-blading and coagulation methods, as described in previous reports.[48,49,62] The diaphragms were sequentially immersed in PVA and glutaraldehyde solutions to form PVA hydrogel overlayer (Fig. S1, SI). The acetal groups (1,3-dioxane-type acetals) formed by the reaction between the hydroxyl groups of PVA and the aldehyde group of glutaraldehyde are known to be chemically stable, even under strong alkaline conditions.[63,64] The concentration of the PVA solution was systematically varied (x wt/v%, where x denotes the PVA concentration) to control the porosity and superaerophobicity of the hydrogel layer. Although our primary focus was on modifying diaphragms for alkaline water electrolyzers, the present method can also be applied to ion-selective membranes used in PEM and AEM electrolyzers.
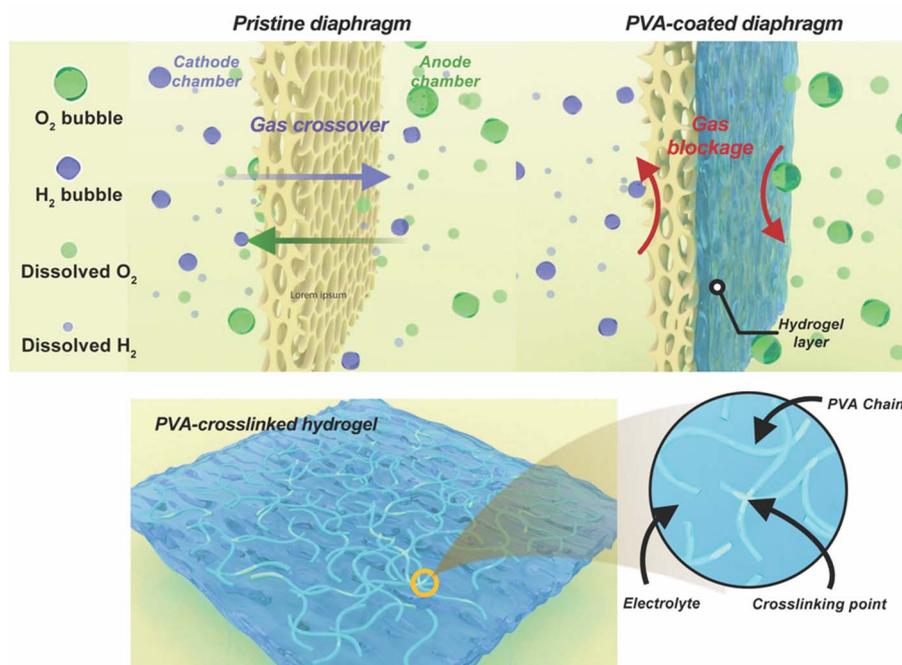
Fig. 1 Schematic illustration showing gas crossover suppression by hydrogel-coated diaphragm. In a pristine diaphragm, both dissolved gases and gas bubbles permeate through pores, leading to crossover between the cathode and anode chambers. In contrast, the hydrogel-coated diaphragm suppresses gas transport by blocking bubble penetration and hindering dissolved gas diffusion. The enlarged view highlights the porous and hydrophilic PVA hydrogel overlayer, where polymer chains are chemically cross-linked via acetal linkages.

Morphological and quantitative analyses were conducted to investigate how PVA concentration influenced the structure and properties of hydrogel. Scanning electron microscopy (SEM) was used to examine the morphology of diaphragms with and without hydrogel modification (Fig. 2b). The pristine diaphragm exhibited a porous structure, consistent with previous
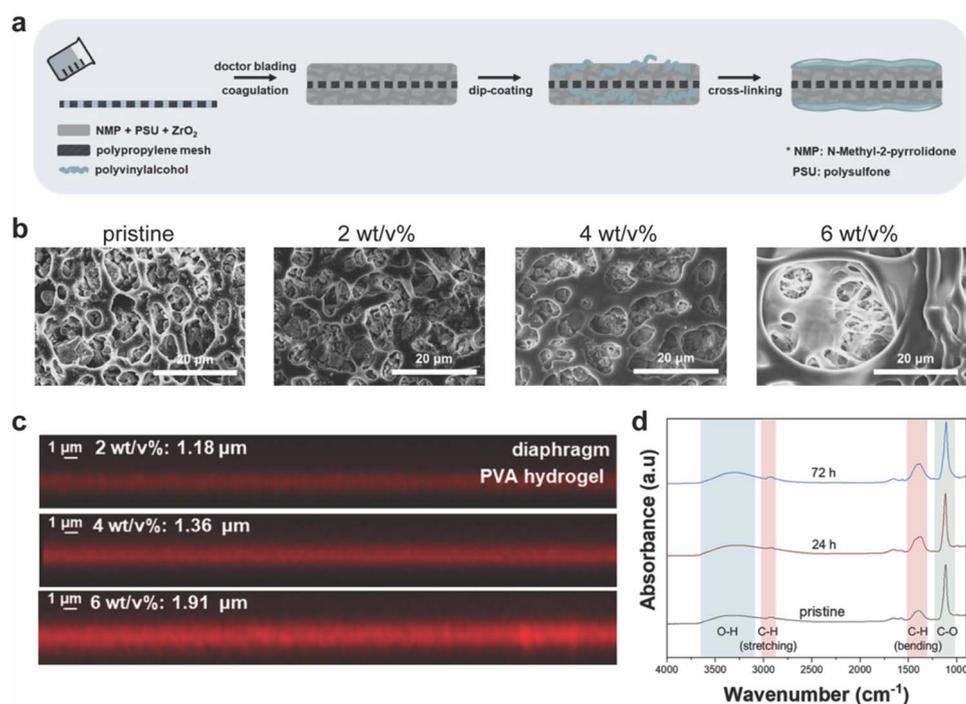

Fig. 2 Fabrication and structural characterization of PVA hydrogel-modified diaphragms. (a) Schematic illustration of the fabrication process of PVA hydrogel-modified diaphragms. (b) SEM images showing morphological changes with increasing PVA concentration. (c) Cross-sectional CLSM images quantifying hydrogel layer thickness. (d) FT-IR spectra of PVA hydrogels after immersion in 30 wt% KOH for 0, 24, and 72 h, confirming the retention of acetal linkages and chemical stability under alkaline conditions.
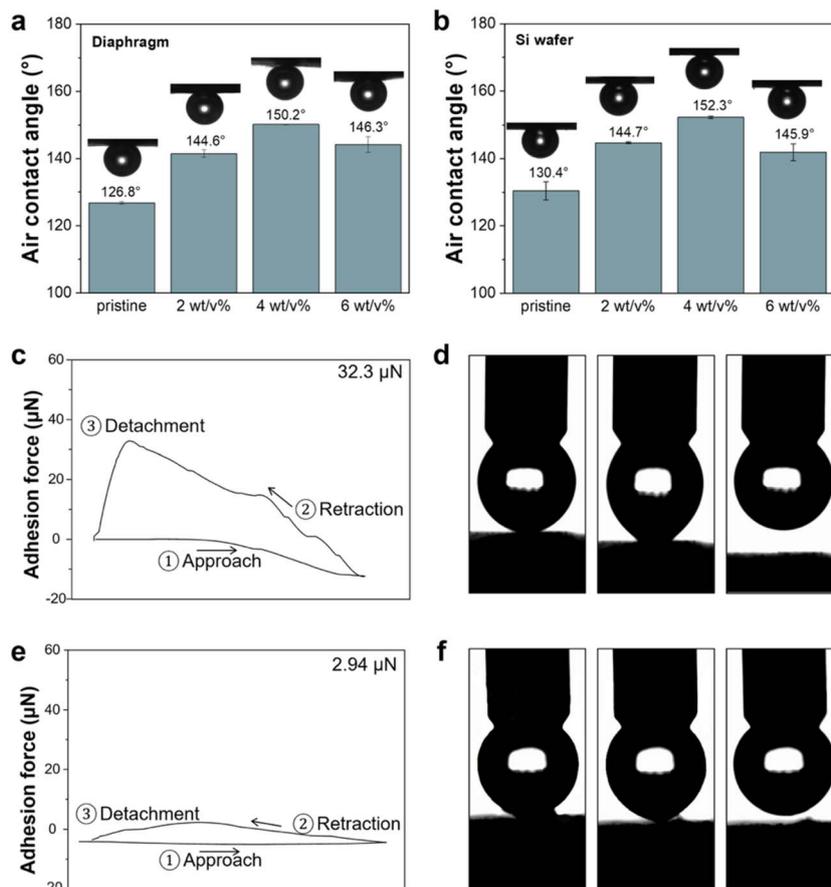
Fig. 3 Superaerophobicity and bubble adhesion of hydrogel-modified diaphragms. (a and b) Air contact angles of PVA hydrogels with different concentrations measured on (a) a diaphragm and (b) a Si wafer. (c–f) Bubble adhesion force measurements and corresponding photographs for (c and d) the pristine and (e and f) the 4 wt/v% hydrogel-coated diaphragms.

reports.[37,49] At 2 wt/v%, the hydrogel displayed loosely connected polymer networks, likely due to insufficient crosslinking at low PVA content. In contrast, the 6 wt/v% sample showed dense polymer aggregation and closed-pore structures, indicative of excessive crosslinking and polymer aggregation. These trends were further corroborated by confocal laser scanning microscopy (CLSM), which quantified the thickness of hydrogel coating (Fig. 2c). The hydrogel-coated layer (red-marked) measured 1.18 μm at 2 wt/v%, increased slightly to 1.36 μm at 4 wt/v%, and then rose sharply to 1.91 μm at 6 wt/v%, consistent with the aggregation and pore blockage observed in SEM.

To evaluate pore size, hydrogels were deposited on flat substrates to eliminate the influence of the diaphragm's intrinsic pores (Fig. S2, SI). At 6 wt/v%, the surface was completely covered by PVA hydrogel with no visible porosity, consistent with the excess concentration. By contrast, the 2 and 4 wt/v% samples retained porous structures, with porosities of 88.09% and 47.51% and average pore sizes of 11.15 μm and 6.33 μm, respectively. Importantly, OH^- conductivity of the diaphragms showed no statistically significant degradation after hydrogel modification, except for the 6 wt/v% samples (Fig. S3, SI), likely due to the relatively high porosity of hydrogels. Overall, SEM, CLSM, OH^- conductivity analyses demonstrate that 4 wt/v% provides the optimal balance between sufficient

crosslinking and minimal aggregation, yielding a uniform and porous hydrogel structure.

The chemical stability of PVA hydrogels under strongly alkaline conditions was evaluated by immersing samples in 30 wt% KOH for different durations and analyzing them using Fourier-transform infrared (FT-IR) spectroscopy. Even after immersing for 24 and 72 h, the hydrogels maintained their chemical structures, including the C–H peak associated with acetal linkages (Fig. 2d), demonstrating the chemical stability of PVA hydrogels under harsh alkaline conditions. In addition, the pristine diaphragm and the 4 wt/v% PVA hydrogel-coated diaphragm were immersed in 30 wt% KOH for 50 h, followed by measurements of the air contact angle and bubble point pressure (BPP). After immersion, the hydrogel-coated diaphragm retained its superaerophobic characteristics, as confirmed by the air contact angle and BPP measurements (Fig. S4, SI). These results indicate that the key interfacial and transport-related properties remained stable after alkaline immersion.

3.2. Superaerophobicity of hydrogel-modified diaphragms

To further investigate the relationship between hydrogel structure and interfacial properties, the superaerophobicity of hydrogel-modified diaphragms was evaluated by measuring the
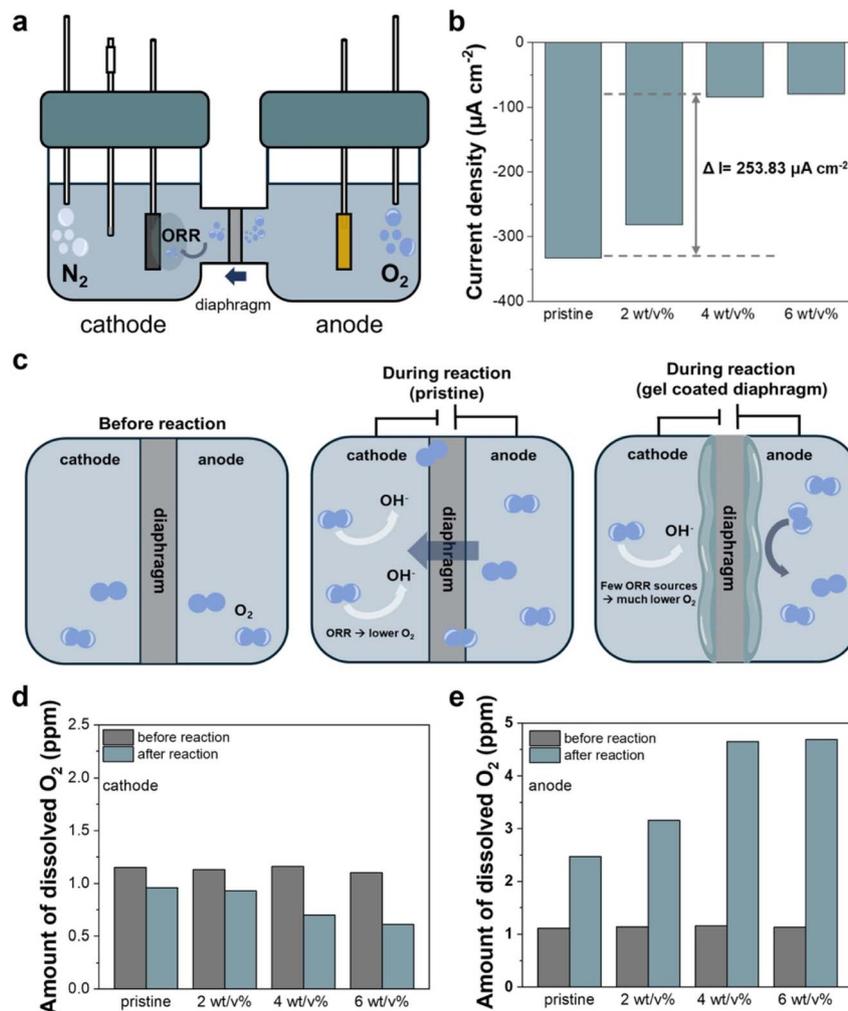
Fig. 4 Evaluation of dissolved oxygen crossover in pristine and hydrogel-coated diaphragms. (a) Schematic illustration of the H-type cell used for oxygen penetration and ORR measurement. (b) Reduction current densities arising from penetrated oxygen, clearly suppressed by hydrogel-coated diaphragms. (c) Schematics of dissolved oxygen crossover before and during electrolysis with pristine and hydrogel-coated diaphragms. (d and e) Dissolved oxygen concentrations in the (d) cathode and (e) anode compartments before and after AWE operation, showing reduced O_2 crossover with hydrogel modification.

air contact angles (θ_{air}) with varying concentrations of PVA. Among the samples, the 4 wt/v% hydrogel exhibited the highest aerophobicity on both the porous diaphragm surface and a flat Si wafer substrate (Fig. 3a and b). Notably, it also demonstrated superaerophobic behavior ($\theta_{air} > 150°$), which can be attributed to its well-balanced crosslinking network. Building on these results, the effect of superaerophobicity on gas–solid interactions was further assessed by measuring bubble adhesion forces for both the pristine diaphragm and the superaerophobic 4 wt/v% sample. The pristine diaphragm exhibited a high adhesion force of 32.3 μN (Fig. 3c), indicating strong bubble attachment to the surface (Fig. 3d). In contrast, the 4 wt/v% hydrogel showed a markedly reduced adhesion force of 2.94 μN (Fig. 3e), approximately 11 times lower than that of the pristine diaphragm, with visibly weaker bubble adhesion (Fig. 3f). This substantial reduction is attributed to the superaerophobic properties of the PVA hydrogel layer. Accordingly, the bubble point pressure (BPP)[65] of diaphragms—the minimum gas

pressure required to force the first continuous stream of bubbles through a wetted membrane—increased upon hydrogel modification (Fig. S5, SI). These results indicate that hydrogel modification can suppress gas crossover by promoting rapid bubble detachment or preventing bubble adhesion during AWE operation.

3.3. Gas crossover tests by quantification of dissolved oxygen

Before testing diaphragms in an AWE, we evaluate their gas crossover behavior by indirectly measuring the relative amount of dissolved oxygen (DO) *via* oxygen reduction reactions (ORR) in an H-cell (Fig. 4a). During the experiment, N_2 and O_2 gases were continuously purged into the working and counter electrode compartments, respectively, and chronoamperometry (CA) was conducted at 0.2 V *vs.* RHE, where ORR—but not hydrogen evolution reaction (HER)—occur. Thus, the current densities in this cell can be used to indirectly compare oxygen crossover across diaphragm (Fig. 4b). The reduction current
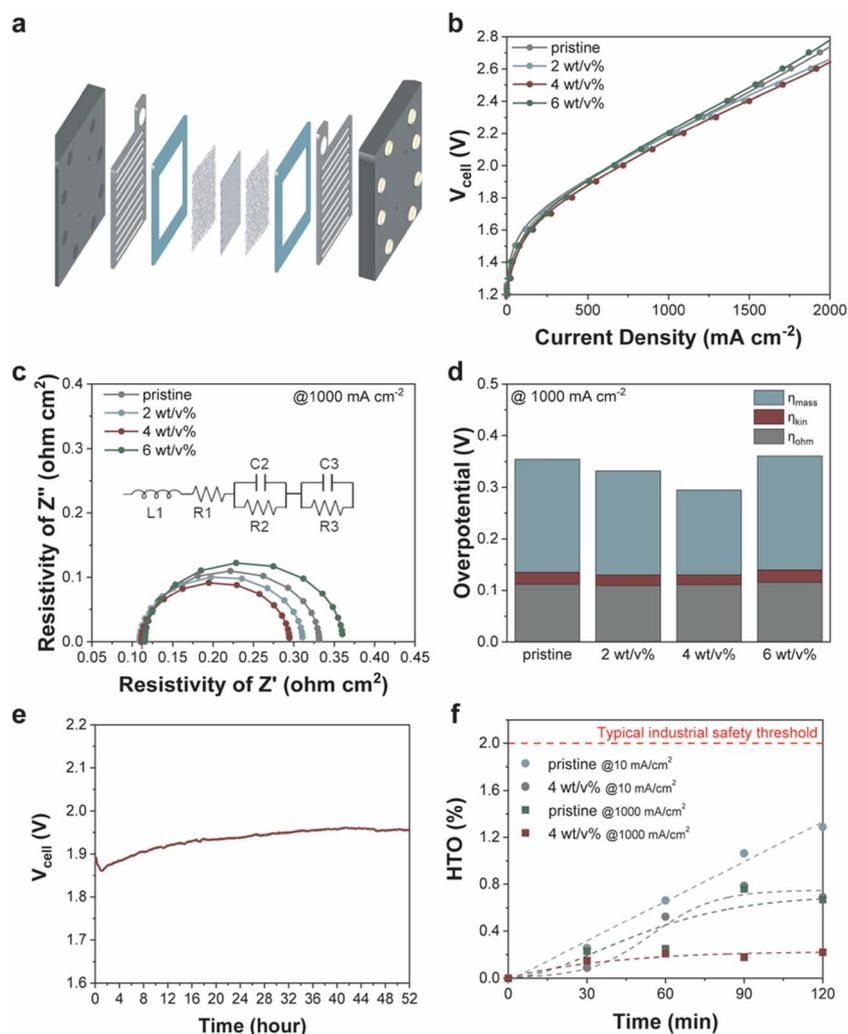
Fig. 5 Electrochemical performance and gas crossover analysis of pristine and hydrogel-coated diaphragms in AWE. (a) Schematic illustration of the MEA cell system used in this study. (b) Polarization curves comparing pristine and hydrogel-coated diaphragms. (c) EIS spectra at 1000 mA cm^{-2}. (d) Overpotential analysis at 1000 mA cm^{-2}, showing reduced mass transport overpotential for the 4 wt/v% hydrogel-coated diaphragm. (e) Cell voltage profile during constant-current AWE operation at 400 mA cm^{-2} for >50 h. (f) Hydrogen-in-oxygen ratio (HTO) calculated from measured H_2 and O_2 concentrations in the gas phase at current densities of 10 and 1000 mA cm^{-2}.

density reached ~330 μA cm^{-2} with the pristine diaphragm. In contrast, hydrogel-coated diaphragms exhibited substantially lower reduction currents due to the suppression of O_2 crossover: ~210, ~70, and ~70 μA cm^{-2} for diaphragms modified with 2, 4, and 6 wt/v% hydrogels, respectively.

Encouraged by these findings, we directly measured DO concentrations in both the anode and cathode compartments of AWEs operated at room temperature with the pristine and hydrogel-coated diaphragms (Fig. 4c). Since O_2 solubility decreases significantly at the practical operation temperature of ~80 °C, these measurements were carried out at room temperature to ensure sufficient sensitivity for detecting dissolved oxygen. Before operation, the initial DO concentrations were similar across all diaphragms, at ~1 ppm. To examine the performance over a broad operating window, electrolysis tests were conducted at both 1000 and 10 mA cm^{-2} for 30 min. The DO concentration in the cathode compartment decreased due to consumption via ORR (Fig. 4d and Fig. S6a, SI), whereas the

DO concentration increased in the anode compartment because of O_2 generation by oxygen evolution reactions (OER) (Fig. 4e and Fig. S6b, SI). Importantly, the hydrogel-coated diaphragm consistently exhibited lower DO levels in the cathode compartment and higher DO levels in the anode compartment compared with the pristine diaphragm at both current densities, demonstrating effective crossover suppression under both low- and high-current operations.

3.4. Electrochemical performance and gas crossover in AWEs with hydrogel-coated diaphragms

The electrochemical performance of hydrogel-modified diaphragms was evaluated using a zero-gap AWEs (Fig. 5a). Ni foam was used to fabricate catalyst-coated substrate (CCS)-type membrane electrode assemblies. As shown in the polarization curves, the 4 wt/v% hydrogel-coated diaphragm exhibited a comparable or slightly higher current density, both with and

without *iR* compensation (Fig. 5b and S7, SI). This behavior is attributed to facilitated bubble removal from the diaphragm and nearby catalyst layers in the zero-gap AWE configuration, enabled by the porous superaerophobic hydrogel layer, which introduces negligible additional ohmic resistance. By contrast, the 6 wt/v% hydrogel led to performance degradation likely due to its lower OH^- conductivity. The performance gap became more pronounced at current densities exceeding 1000 mA cm^{-2}, consistent with reduced mass transport overpotentials from accelerated bubble detachment. Electrochemical impedance spectroscopy (EIS) supports this interpretation: at 1000 mA cm^{-2}, the 4 wt/v% hydrogel exhibited the lowest total overpotential, with a 54.4 mV reduction in mass transport overpotential relative to the pristine diaphragm, while ohmic and kinetic overpotentials remained similar (Fig. 5c and d). To further assess durability under operation, we conducted an extended constant-current stability test at 400 mA cm^{-2}. The cell voltage remained stable over 50 h, showing only a gradual increase from 1.89 V at the beginning to 1.96 V after 52 h (Fig. 5e).

In situ H_2 crossover was next evaluated by gas chromatography (GC) analysis of the anode gas phase, and the results are reported as HTO ratios, which are a key safety metric for industrial alkaline water electrolysis. Accordingly, GC-based measurements of the hydrogen concentration in the oxygen stream were performed at 10 mA cm^{-2}, representing low-load operation where gas crossover can become critical,[42] and at 1000 mA cm^{-2}, corresponding to a commercially relevant operating condition. At both current densities, the hydrogel-modified diaphragms exhibited lower HTO values than the pristine ones (Fig. 5f). Notably, at the low current density of 10 mA cm^{-2}, the HTO values for the pristine diaphragm increased almost linearly and reached 1.29% after 2 h, whereas the 4 wt/v% hydrogel-coated diaphragm showed rapid saturation at a much lower value (0.69% after 2 h). These results further confirm that gas crossover becomes more pronounced at lower current densities, consistent with previous reports.[40–42] Importantly, the HTO values under both operating conditions remained well below the commonly applied safety threshold for electrolyzer operation (2 vol%),[44] confirming safe operation of the AWE system. Compared with the pristine diaphragm, the 4 wt/v% PVA hydrogel-coated diaphragm achieved crossover suppression rates of 46.4% at 10 mA cm^{-2} and 67.2% at 1000 mA cm^{-2} (Fig. S8, SI). These results demonstrate that the hydrogel coating effectively suppresses hydrogen crossover across a broad operating window, including both low-load conditions relevant to renewable energy operation and high-current industrial operation.

To examine the general applicability of this approach, PVA hydrogel was also coated on a PiperION membrane for AEM water electrolysis using the same dip-coating protocol (Fig. S9, SI). Compared with the pristine AEM, the 4 wt/v% PVA hydrogel-coated AEM exhibited reduced hydrogen crossover into the anode gas phase, attributed to faster bubble detachment induced by its superaerophobicity. Collectively, these findings demonstrate that superaerophobic PVA hydrogel coatings effectively suppress gas crossover in both diaphragms for alkaline water electrolyzers and anion exchange membranes for AEM water electrolyzers.

3.5. *In situ* observation of hydrogen bubble behavior

To complement the gas crossover measurements, hydrogen bubble behavior between the cathode and diaphragm was visualized for both the pristine and 4 wt/v% samples using a custom-designed cell (Fig. 6, Movies S1 and S2, SI). A 200 μm gap was maintained between the diaphragm and cathode to enable observation under operating conditions. With the pristine diaphragm, significant bubble accumulation was observed. At 33.3 s, hydrogen gas bubbles adhered to the diaphragm surface, and smaller bubbles accumulated on them, leading to coalescence and growth. By 60 s, the bubbles had grown substantially and eventually detached at 67 s, when the buoyancy forces overcame adhesion force. In contrast, with 4 wt/v% hydrogel-coated diaphragm, bubbles detached rapidly or failed to adhere altogether, indicating efficient gas release facilitated by the superaerophobic hydrogel surface. These visual observations are consistent with earlier gas crossover results, where the 4 wt/v% coating effectively suppressed gas crossover.

Collectively, these findings highlight the critical role of interfacial bubble dynamics in governing gas crossover during alkaline water electrolysis. The superaerophobic hydrogel coating, fabricated *via* a simple and scalable dip-coating process, enabled rapid gas bubble release, thereby mitigating gas crossover and associated mass transport losses. High-speed imaging and interfacial force analyses verified the effectiveness of the superaerophobic surface in minimizing bubble adhesion. Overall, these results emphasize the importance of interfacial wettability in diaphragm design and demonstrate a practical, durable approach to suppressing gas crossover and operational safety in AWE systems. Nevertheless, these experiments were conducted under well-controlled laboratory-scale conditions,
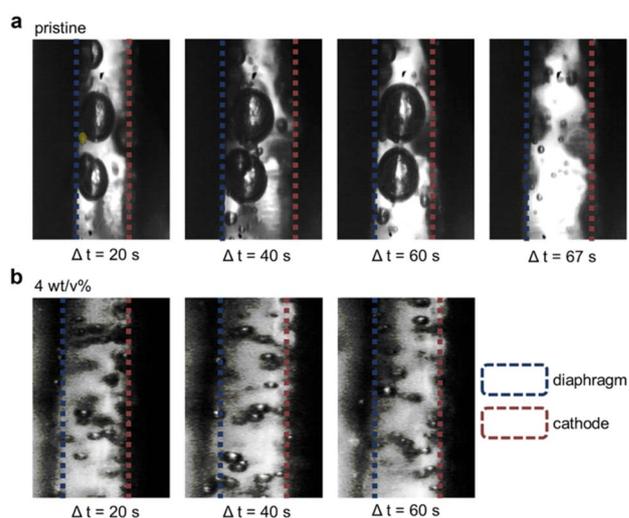

Fig. 6 *In situ* observation of hydrogen bubble dynamics with pristine and hydrogel-coated diaphragms. Time-lapse images showing bubble accumulation, coalescence, and delayed detachment on (a) the pristine diaphragm, compared with rapid detachment and minimal adhesion on (b) the 4 wt/v% hydrogel-coated diaphragm.

and the long-term durability of the hydrogel coating under dynamic operating environments remains to be fully validated. Further studies should assess coating stability under fluctuating current densities and in large-area electrode systems to advance this approach toward industrial application.

3.6. Comparison with previous diaphragm-modification strategies

Although previous diaphragm-modification studies aimed at suppressing gas crossover have proposed a variety of material designs and surface or structural control strategies, they often suffer from limited manufacturability and scalability due to complex fabrication processes (Table S1, SI). Such limitations can hinder translation into practical AWE systems and may delay the industrial adoption of separator modification technologies intended to enhance operational safety. In contrast, the PVA hydrogel-based dip-coating approach proposed in this work offers a simple and scalable process that can be readily applied to commercial separators. This strategy demonstrates a practical alternative that enables effective control of interfacial wettability and gas behavior without requiring complicated fabrication procedures.

Another common limitation in prior studies is that, despite targeting gas crossover mitigation, direct quantification of gas crossover under realistic AWE operating conditions has often been limited. Many previous reports have relied primarily on indirect membrane–property indicators, such as bubble-point pressure (BPP) and contact-angle measurements. In this study, beyond membrane–property characterization, we directly quantified gas crossover using several operation-relevant evaluations, including *in situ* gas-phase composition analysis by gas chromatography (GC) during AWE operation, dissolved oxygen (DO) quantification during operation, and penetrated-oxygen assessment *via* H-cell-based ORR measurements. These results demonstrate that the proposed approach not only improves interfacial properties but also can translate into measurable reductions in gas crossover at the system level, thereby enhancing the operational safety of AWE system.

4. Conclusions

We developed a superaerophobic PVA hydrogel-coated diaphragm using a simple and scalable dip-coating method to suppress gas crossover in AWEs. The superaerophobic hydrogel coating not only mitigated gas crossover but also effectively reduced mass transport overpotential by promoting rapid bubble detachment during AWE operation. Bubble adhesion force measurements and high-speed imaging confirmed this enhanced gas bubble release, attributed to the superaerophobic nature of the hydrogel surface. Both direct and indirect quantitative analyses further demonstrated significant suppression of gas crossover with the hydrogel-coated diaphragm. Overall, this study identifies the surface wettability of the diaphragm as a critical factor for operational safety and introduces a scalable, practical strategy for improving hydrogen production efficiency through hydrogel-based surface engineering.

Author contributions

Conflicts of interest

There are no conflicts to declare.

Data availability

The data supporting the findings of this study are available within the article and its supplementary information (SI). Supplementary information: additional experimental details, characterization data, supplementary figures, and supporting analysis related to the hydrogel-coated diaphragm and gas crossover behavior. Please include this description in the data availability statement. See DOI: https://doi.org/10.1039/d5ta07926h.

Acknowledgements

References

1 M. Nasser, T. F. Megahed, S. Ookawara and H. Hassan, *Environ. Sci. Pollut. Res.*, 2022, **29**, 86994–87018.

2 A. Franco and C. Giovannini, *Sustainability*, 2023, **15**, 16917.

3 R. R. Beswick, A. M. Oliveira and Y. Yan, *ACS Energy Lett.*, 2021, **6**, 3167–3169.

4 M. Chatenet, B. Pollet, D. Dekel, F. Dionigi, J. Deseure, P. Millet, R. Braatz, M. Bazant, M. Eikerling, I. Staffell, P. Balcombe, Y. Shao-Horn and H. Schäfer, *Chem. Soc. Rev.*, 2022, **51**, 4583–4762.

5 M. Awad, A. Said, M. Saad, A. Farouk, M. M. Mahmoud, M. Alshammari, M. Alghaythi, S. Abdel Aleem, A. Abdelaziz and A. Omar, *Alexandria Eng. J.*, 2024, **87**, 213–239.

6 S. Shiva Kumar and H. Lim, *Energy Rep.*, 2022, **8**, 13793–13813.

7 S. Sharma, S. Agarwal and A. Jain, *Energies*, 2021, **14**, 7389.

8 N. Rambhujun, M. S. Salman, T. Wang, C. Pratthana, P. Sapkota, M. Costalin, Q. Lai and K.-F. Aguey-Zinsou, *MRS Energy Sustain.*, 2020, **7**, 33.

9 P. J. Megía, A. J. Vizcaíno, J. A. Calles and A. Carrero, *Energy Fuels*, 2021, **35**, 16403–16415.

10 N. Danilovic, R. Subbaraman, K.-C. Chang, S. H. Chang, Y. J. Kang, J. Snyder, A. P. Paulikas, D. Strmcnik, Y.-T. Kim, D. Myers, V. R. Stamenkovic and N. M. Markovic, *J. Phys. Chem. Lett.*, 2014, **5**, 2474–2478.

11 N. Du, C. Roy, R. Peach, M. Turnbull, S. Thiele and C. Bock, *Chem. Rev.*, 2022, **122**, 11830–11895.

12 E. Hong, Z. Yang, H. Zeng, L. Gao and C. Yang, *ACS Energy Lett.*, 2024, **6**, 1623–1648.

13 D. Henkensmeier, W.-C. Cho, P. Jannasch, J. Stojadinovic, Q. Li, D. Aili and J. O. Jensen, *Chem. Rev.*, 2024, **124**, 6393–6443.

14 N. V. Kuleshov, V. N. Kuleshov, S. Kurochkin, A. A. Gavrilyuk and V. Tyutrina, *Modern High Technologies*, 2022, **1**, 94–99.

15 S. Sebbahi, A. Assila, A. Alaoui Belghiti, S. Laasri, S. Kaya, E. K. Hlil, S. Rachidi and A. Hajjaji, *Int. J. Hydrogen Energy*, 2024, **82**, 583–599.

16 Q. Cai, W. Hong, C. Jian, X. He and W. Liu, *Adv. Energy Sustainability Res.*, 2023, **4**, 2200178.

17 A. L. Rangel-Cárdenas and G. J. M. Koper, *Materials*, 2017, **10**, 576.

18 M. Segale, T. Seadira, R. Sigwadi, T. Mokrani and G. Summers, *Mater. Adv.*, 2024, **5**, 7979–8006.

19 M. Khan, X. Li, J. Garcia, M. Lashari, A. ur rehman, N. Elboughdiri, L. Kolsi and D. Ghernaout, *ACS Omega*, 2021, **6**, 7994–8001.

20 C. R. Peltier, W. You, D. Fackovic Volcanjk, Q. Li, A. J. Macbeth, H. D. Abruña and G. W. Coates, *ACS Energy Lett.*, 2023, **8**, 2365–2372.

21 C. R. Wang, J. M. Stansberry, R. Mukundan, H.-M. J. Chang, D. Kulkarni, A. M. Park, A. B. Plymill, N. M. Firas, C. P. Liu, J. T. Lang, J. K. Lee, N. E. Tolouei, Y. Morimoto, C. H. Wang, G. Zhu, J. Brouwer, P. Atanassov, C. B. Capuano, C. Mittelsteadt, X. Peng and I. V. Zenyuk, *Chem. Rev.*, 2025, **125**, 1257–1302.

22 T. Ferriday, S. Nuggehalli Sampathkumar, P. Middleton, M. Kolhe and J. Van Herle, *Int. J. Energy Res.*, 2024, **2024**, 7856850.

23 F. Razmjooei, T. Morawietz, E. Taghizadeh, E. Hadjixenophontos, L. Mues, M. Gerle, B. D. Wood, C. Harms, A. S. Gago, S. A. Ansar and K. A. Friedrich, *Joule*, 2021, **5**, 1776–1799.

24 M. Muhyuddin, C. Santoro, L. Osmieri, V. C. A. Ficca, A. Friedman, K. Yassin, G. Pagot, E. Negro, A. Konovalova, G. Lindquist, L. Twight, M. Kwak, E. Berretti, V. D. Noto, F. Jaouen, L. Elbaz, D. R. Dekel, P. Mustarelli, S. W. Boettcher, A. Lavacchi and P. Atanassov, *Chem. Rev.*, 2025, **125**, 6906–6976.

25 P. Trinke, B. Bensmann and R. Hanke-Rauschenbach, *Int. J. Hydrogen Energy*, 2017, **42**, 14355–14366.

26 H. Araújo, J. Gomez and D. Santos, *Catalysts*, 2024, **14**, 845.

27 J. Lei, Z. Wang, Y. Zhang, M. Ju, H. Fei, S. Wang, C. Fu, X. Yuan, Q. Fu, M. U. Farid, H. Kong, A. K. An, R. Deng, F. Liu and J. Wang, *Carbon Neutrality*, 2024, **3**, 25.

28 S. A. Lee, J. Kim, K. C. Kwon, S. Park and H. Jang, *Carbon Neutralization*, 2022, **1**, 26–48.

29 M. Mandal, *ChemElectroChem*, 2021, **8**, 36–45.

30 K. Yassin, R. Attias, Y. Tsur and D. R. Dekel, *ACS Electrochem.*, 2025, **1**, 655–666.

31 H. Zhang, Y. Zuo and J. Huang, *Chem. Synth.*, 2025, **5**, 52.

32 J. Kown, S. Choi, C. Park, H. Han and T. Song, *Mater. Chem. Front.*, 2023, **8**, 41–81.

33 J. Ehlers, A. Feidenhans'l, K. Therkildsen and G. Larrazábal, *ACS Energy Lett.*, 2023, **8**, 1502–1509.

34 C. Daoudi and T. Bounahmidi, *Int. J. Hydrogen Energy*, 2024, **49**, 646–667.

35 J. Brauns and T. Turek, *Processes*, 2020, **8**, 248.

36 P. Trinke, P. Haug, J. Brauns, B. Bensmann, R. Hanke-Rauschenbach and T. Turek, *J. Electrochem. Soc.*, 2018, **165**, F502.

37 H. I. Lee, D. Dung, J. Kim, J. H. Pak, S. Kim, H.-S. Cho, W. Cho and C.-H. Kim, *Int. J. Energy Res.*, 2019, **44**, 1875–1885.

38 M. Schalenbach, W. Lueke and D. Stolten, *J. Electrochem. Soc.*, 2016, **163**, F1480–F1488.

39 M. Schalenbach, G. Tjarks, M. Carmo, W. Lueke, M. Mueller and D. Stolten, *J. Electrochem. Soc.*, 2016, **163**, F3197–F3208.

40 R. Lira Garcia Barros, J. T. Kraakman, C. Sebregts, J. van der Schaaf and M. T. de Groot, *Int. J. Hydrogen Energy*, 2024, **49**, 886–896.

41 M. T. de Groot, J. Kraakman and R. L. Garcia Barros, *Int. J. Hydrogen Energy*, 2022, **47**, 34773–34783.

42 B. Rausch, M. D. Symes, G. Chisholm and L. Cronin, *Science*, 2014, **345**, 1326–1330.

43 M. Muthiah, M. Elnashar, W. Afzal and H. Tan, *Int. J. Hydrogen Energy*, 2024, **84**, 803–821.

44 J. W. Lee, J. H. Lee, C. Lee, H.-S. Cho, M. Kim, S.-K. Kim, J. H. Joo, W.-C. Cho and C.-H. Kim, *Chem. Eng. J.*, 2022, **428**, 131149.

45 Y. Zuo, S. Bellani, M. Ferri, G. Saleh, D. Shinde, M. Zappia, R. Brescia, M. Prato, L. De Trizio, I. Infante, F. Bonaccorso and L. Manna, *Nat. Commun.*, 2023, **14**, 4680.

46 R. B. Patil, M. Kaur, S. D. House, L. Kavalsky, K. Hu, S. Zhong, D. Krishnamurthy, V. Viswanathan, J. Yang, Y. Yan, J. Lattimer and J. R. McKone, *Energy Adv.*, 2023, **2**, 1500–1511.

47 B. Chang, X. Liu, S. Zuo, Y. Ren, J. He, D. Wang, Y. Lei, M. Hu, W.-L. Li, M. A. Khan, R. Aleisa, R. Hu, Y. Hou, H. Liu, W. Zhou, Z. Lai, H. N. Alshareef and H. Zhang, *Nat. Commun.*, 2025, **16**, 7959.

48 P. Vermeiren, R. Leysen, H. Beckers, J. Moreels and A. Claes, *J. Porous Mater.*, 2008, **15**, 259–264.

49 H. I. Lee, M. Mehdi, S. Kim, H.-S. Cho, M. Kim, W. Cho, Y. Rhee and C.-H. Kim, *J. Membr. Sci.*, 2020, **616**, 118541.

50 X. Luo, N. Xu, Y. Zhou, X. Yang, W. Yang, G. Liu, J. K. Lee and J. Qiao, *eScience*, 2024, **4**, 100290.

51 K. Wang, X. Zhang, C. Li, X. Sun, Q. Meng, Y. Ma and Z. Wei, *Adv. Mater.*, 2015, **27**, 7451–7457.

52 Z. Zhu, Y. Lin, P. Fang, M. Wang, M. Zhu, X. Zhang, J. Liu, J. Hu and X. Xu, *Adv. Mater.*, 2024, **36**, 2307035.

53 X. Lu and C. Zhao, *Nat. Commun.*, 2015, **6**, 6616.

54 C. Song, L. Min, W. Zhang, L. Xu and Y. Wang, *J. Membr. Sci.*, 2023, **683**, 121883.

55 D. Martinho and T. Berning, *Membranes*, 2025, **15**, 206.

56 D. Jeon, J. Park, C. Shin, H. Kim, J.-W. Jang, D. Lee and J. Ryu, *Sci. Adv.*, 2020, **6**, eaaz3944.

57 M. Bae, Y. Kang, D. W. Lee, D. Jeon and J. Ryu, *Adv. Energy Mater.*, 2022, **12**, 2201452.

58 J. Park, D. Jeon, Y. Kang, J. Ryu and D. W. Lee, *J. Mater. Chem. A*, 2023, **11**, 1658–1665.

59 Y. Kang, S. Lee, S. Han, D. Jeon, M. Bae, Y. Choi, D. W. Lee and J. Ryu, *Adv. Funct. Mater.*, 2024, **34**, 2308827.

60 Y. Kang, S. Lee, J. Lee, S. Lee, G. Lee, H. Kim, G. H. Choi, J. Ryu and D. W. Lee, *Adv. Sci.*, 2026, **13**, e08569.

61 L. Liu, A. Chakma and X. Feng, *J. Membr. Sci.*, 2008, **310**, 66–75.

62 H. Qin, J. Li, G. Lin, K. Yuan, H. Yang, Y. Ye, T. Jin, F. Cheng and L. Jiao, *Adv. Mater.*, 2025, **37**, 2507573.

63 Y. Li and S. Yao, *Polym. Degrad. Stab.*, 2017, **137**, 229–237.

64 P.-Y. Hsu, T.-Y. Hu, S. R. Kumar, C.-H. Chang, K. C. W. Wu, K.-L. Tung and S. J. Lue, *Polymers*, 2018, **10**, 102.

65 Y. Liao, G. Deng, L. Ding and H. Wang, *J. Membr. Sci.*, 2024, **689**, 122182.